A study of valproic acid for patients with spinal muscular atrophy.	Saito T, Nurputra DK, Harahap NI, Harahap IS, Yamamoto H, Muneshige E, Nishizono H, Matsumura T, Fujimura H, Sakoda S, Saito K, NishioH.	Neurol Clin Neurosci.	2014	国外
Clinical features of Duchenne muscular dystrophy aged over 40 years.	Saito T, Kawai M, Matsumura T, Fujimura H, Sakoda S.	Neuromuscul Disord.	2014	国外
A trial of hybrid assistive limb (HAL) for a spinal muscular atrophy (SMA) patient.	Iwata Y, Saito T, Nagayama H, Yamamoto H, Nishizono H, Shibuichi K, Inoue K, Fujimura H, Nakajima T.	Neuromuscul Disord.	2014	国外
Coagulation and Fibrinolysis Abnormalities in Patients with Muscular Dystrophy.	Saito T.	Fibrinolysis and Thrombolysis Edited by Krasimir Kolev.Intech.	2014	国外

Ⅳ. 研究成果の刊行物・別冊

Stem Cell Reports
Report
ISSCR
OPEN ACCESS

Generation of Alveolar Epithelial Spheroids via Isolated Progenitor Cells from Human Pluripotent Stem Cells

Shimpei Gotoh,[1,*] Isao Ito,[1,2,*] Tadao Nagasaki,[1] Yuki Yamamoto,[1] Satoshi Konishi,[1] Yohei Korogi,[1] Hisako Matsumoto,[1] Shigeo Muro,[1] Toyohiro Hirai,[1] Michinori Funato,[3] Shin-Ichi Mae,[3] Taro Toyoda,[3] Aiko Sato-Otsubo,[4] Seishi Ogawa,[4] Kenji Osafune,[3] and Michiaki Mishima[1]
[1]Department of Respiratory Medicine, Graduate School of Medicine
[2]Institute for Integrated Cell-Material Sciences (iCeMS)
[3]Center for iPS Cell Research and Application (CiRA)
[4]Department of Pathology and Tumor Biology, Graduate School of Medicine
Kyoto University, Kyoto 606-8507, Japan
*Correspondence: a0009650@kuhp.kyoto-u.ac.jp (S.G.), isaoito@kuhp.kyoto-u.ac.jp (I.I.)
http://dx.doi.org/10.1016/j.stemcr.2014.07.005

SUMMARY

No methods for isolating induced alveolar epithelial progenitor cells (AEPCs) from human embryonic stem cells (hESCs) and induced pluripotent stem cells (hiPSCs) have been reported. Based on a study of the stepwise induction of alveolar epithelial cells (AECs), we identified carboxypeptidase M (CPM) as a surface marker of NKX2-1$^+$ "ventralized" anterior foregut endoderm cells (VAFECs) in vitro and in fetal human and murine lungs. Using *SFTPC-GFP* reporter hPSCs and a 3D coculture system with fetal human lung fibroblasts, we showed that CPM$^+$ cells isolated from VAFECs differentiate into AECs, demonstrating that CPM is a marker of AEPCs. Moreover, 3D coculture differentiation of CPM$^+$ cells formed spheroids with lamellar-body-like structures and an increased expression of surfactant proteins compared with 2D differentiation. Methods to induce and isolate AEPCs using CPM and consequently generate alveolar epithelial spheroids would aid human pulmonary disease modeling and regenerative medicine.

INTRODUCTION

Type II alveolar epithelial cells (AECs) are a major cellular component of the distal lung epithelium, where they secrete pulmonary surfactant and generate type I AECs that cover most of the surface area of the alveoli (Whitsett et al., 2010; Rock and Hogan, 2011). The stepwise differentiation of human pluripotent stem cells (hPSCs), including human embryonic stem cells (hESCs) and induced pluripotent stem cells (hiPSCs), into lung epithelial cells would help to elucidate the etiologies of human lung diseases and create novel treatments, and has been reported in both proximal airway cells (Mou et al., 2012; Wong et al., 2012; Firth et al., 2014) and distal lung epithelial cells (Green et al., 2011; Ghaedi et al., 2013; Huang et al., 2014). Currently, however, there are no surface markers that can be used to purify human NKX2-1$^+$ "ventralized" anterior foregut endoderm cells (VAFECs) as alveolar epithelial progenitor cells (AEPCs), although NKX2-1 is an early marker of lung and thyroid development (Kimura et al., 1996). Here, we report the efficacy of carboxypeptidase M (CPM) as a surface marker of AEPCs for generating type II AECs.

RESULTS

Identification of CPM as a Marker of NKX2-1$^+$ VAFECs

We hypothesized that identifying a surface marker for NKX2-1$^+$ VAFECs would be helpful for isolating a homogeneous population of AEPCs without establishing *NKX2-1* reporter cell lines. We constructed a stepwise protocol to induce hPSCs to AECs (Figure 1A). On day 0, previously established hPSCs were seeded (Thomson et al., 1998; Takahashi et al., 2007; Nakagawa et al., 2008; Okita et al., 2013) following single-cell enzymatic dissociation (Kajiwara et al., 2012), resulting in definitive endodermal cells (DECs) at an efficiency of $\geq$80% (Figure S1A available online). In step 2, the DECs were differentiated to anterior foregut endodermal cells (AFECs) (Green et al., 2011) at an efficiency of $\geq$88% (Figure S1B). In step 3, the concentrations of all-*trans* retinoic acid, CHIR99021, and BMP4 were optimized for seven hPSC lines for differentiation into NKX2-1$^+$FOXA2$^+$ cells, attaining an efficiency of 57.0%–77.5% (Figures 1C and 1D; Supplemental Experimental Procedures). In step 4, cells were cultured in medium containing FGF10 for 7 days. In step 5, the cells were differentiated in medium containing dexamethasone, 8-Br-cAMP, 3-isobutyl-1-methylxanthine, and KGF (Gonzales et al., 2002; Longmire et al., 2012). We confirmed induction of AECs by detecting *SFTPB* and *SFTPC* using RT-PCR and double staining SFTPC and SFTPB with NKX2-1 (Figures S1C and S1D). Transcription factors were analyzed by quantitative RT-PCR (qRT-PCR; Figure 1B). *SOX17*, *FOXA2*, *GATA6*, and *SOX2* were compatibly changed on day 6 and day 10 as previously described (Green et al., 2011). On day 14, *NKX2-1*, *GATA6*, *ID2*, *SOX9*, and *HOPX* levels

simultaneously increased. Interestingly, *NKX2-1*, *GATA6*, and *HOPX* levels decreased on day 21 and then increased again on day 25. The levels of other organ lineage markers were found to be limited from day 0 to day 25 (Figure S1E).

In order to identify candidate markers of VAFECs, we performed a microarray analysis to compare the global gene-expression patterns of AFECs (day 10) and VAFECs (day 14) in 201B7 hiPSCs. *CPM* and *NKX2-1* were remarkably upregulated on day 14 (Figures 1E and S1F). In immunofluorescence (IF) staining, CPM and NKX2-1 increased from day 10 to day 14 (Figure 1F), whereas EPCAM and FOXA2 did not appear to change (Figure S1G). Although CPM was reported to be a marker of type I AECs (Nagae et al., 1993), only *CPM* drastically increased on day 14 in a similar pattern to *NKX2-1*, in contrast to other markers of type I AECs (*AQP5* and *CAV1*) (Figure S1H). On day 25, the various airway markers, including distal lung transcription factors (SOX9 and NKX2-1), type II AEC markers (SFTPB and SFTPC), and a club cell marker (SCGB3A2), were expressed in the CPM^+ cells. KRT5, a marker of basal cells, was not expressed in the CPM^+ cells (Figure 1G).

In fetal human lung at 18.5 weeks of gestation, SFTPC and T1α were expressed separately (Figure S1I), while CPM was expressed in $NKX2\text{-}1^+$, $SFTPC^+$, and $T1\alpha^+$ cells (Figure 1H), thus indicating that CPM is expressed in both type I and II AECs in the fetus. The sequential expression of CPM was confirmed in $NKX2\text{-}1^+$ cells of fetal murine lungs at embryonic day 12.5 (E12.5), E15.5, and E17.5 (Figure 1I). For thyroid lineage cells, which differentiated from $NKX2\text{-}1^+$ VAFECs, CPM was found to be negative in both $NKX2\text{-}1^+$ cells and $PAX8^+$ epithelial cells, but weakly positive in $PECAM^+$ endothelial cells in the adult human samples (Figure S1J). In E17.5 fetal and adult murine thyroids, CPM was also negative in $NKX2\text{-}1^+$ and $PAX8^+$ cells (Figure S1K), suggesting that CPM is a lung-lineage marker of VAFECs.

Isolation of $NKX2\text{-}1^+$ VAFECs Using Anti-CPM^+ Antibody

As CPM is a membrane-bound surface protein, we performed flow cytometry with anti-EPCAM and anti-CPM antibodies after dissociating VAFECs on day 14 (Figures 2A and S2A). We then sorted $EPCAM^+CPM^+$ and $EPCAM^+CPM^-$ cells and examined the global gene-expression patterns of these two populations using microarrays. We screened 560 probes with a false discovery rate (FDR)-adjusted p value of <0.05 among 54,675 probes. Gene clustering was performed in 336 probes that differed between the $EPCAM^+CPM^+$ and $EPCAM^+CPM^-$ cells with a fold change (FC) cutoff value of 2.0 (Figures 2B and S2B). Of the clustered genes with the highest expression in the $EPCAM^+CPM^+$ cells, *CPM* ranked among the top five probes with a log FC of >6, as expected. Importantly, the log FCs of two probes for *NKX2-1* were 4.89 and 4.82, respectively. *FOXA1*, *FOXA2*, *HOPX*, and *GATA6* were also included in the list of upregulated genes with log FCs of 3.79, 3.06, 3.61, and 3.29, respectively. Next we sorted the CPM^+ cells using a magnet-activated cell sorting (MACS) system to increase the yield, as almost all of the CPM^+ cells were $EPCAM^+$ cells (96.7% ± 2.1% of CPM^+ cells; Figure 2A). After MACS-based sorting, the proportion of CPM^+ cells in three populations (presorting, positive selection, and negative selection) was 63.4% ± 5.8%, 98.8% ± 0.4%, and 34.0% ± 7.8%, respectively, by flow cytometry (Figure 2C). We then evaluated the proportion of positive $NKX2\text{-}1^+$ cells among the MACS-sorted CPM^+ and CPM^- cells using IF staining (93.0% ± 1.0% versus 29.0% ± 1.0%; Figure S2C) and flow cytometry (92.3% ± 0.7% versus 22.2% ± 2.3%; Figure S2D). Because a portion of the CPM^+ cells appeared to be sorted according to MACS-based CPM negative selection, we investigated the average proportion of $NKX2\text{-}1^+$ cells among the fluorescence-activated cell sorting (FACS)-sorted CPM^+ and CPM^- cells using IF staining (89.9% ± 0.4% versus 4.5% ± 1.7%; Figure 2D). Following CPM-based purification on day 14, *CPM* increased significantly from 0.74-fold ± 0.12-fold to 4.94-fold ± 0.51-fold of that observed in the fetal human lung (n = 5), while *NKX2-1* increased from 0.41-fold ± 0.10-fold to 1.95-fold ± 0.36-fold (n = 5) on qRT-PCR (Figure 2E). We then applied this method to purify AECs on day 25. *CPM*, *NKX2-1*, *SFTPA2*, *SFTPB*, *SFTPC*, *DCLAMP*, *SCGB1A1*, and *SCGB3A2* were significantly increased in the CPM^+ cells (n = 5); however, the level of *SFTPC* was extremely low compared with that observed in the fetal lung. *NGFR*, a marker of proximal airway basal stem cells (Rock et al., 2009), was significantly decreased in the CPM^+ cells (n = 5; Figure 2F).

Generation of *SFTPC-GFP* Knockin Reporter hPSCs

In order to investigate whether CPM is a potential surface marker of AEPCs, we generated *SFTPC-GFP* knockin reporter hPSC lines from 201B7 hiPSCs using BAC-based homologous recombination methods (Mae et al., 2013; Figure 3A; Supplemental Experimental Procedures), as SFTPC is the most specific marker of type II AECs. Following electroporation of the targeting vectors, 12 of 55 G418-resistant clones were found to have a heterozygous deletion of the genomic endogenous *SFTPC*-coding region (Figure 3B). The *pgk-Neo* cassette was removed via electroporation of the Cre-expression vector (Figure 3C), and normal karyotypes of the A17-14 and B2-3 clones were confirmed (Figure S3). The genomic copy number was calculated as previously described (Mae et al., 2013). The parental 201B7 (data not shown), A17-14, and B2-3 clones have

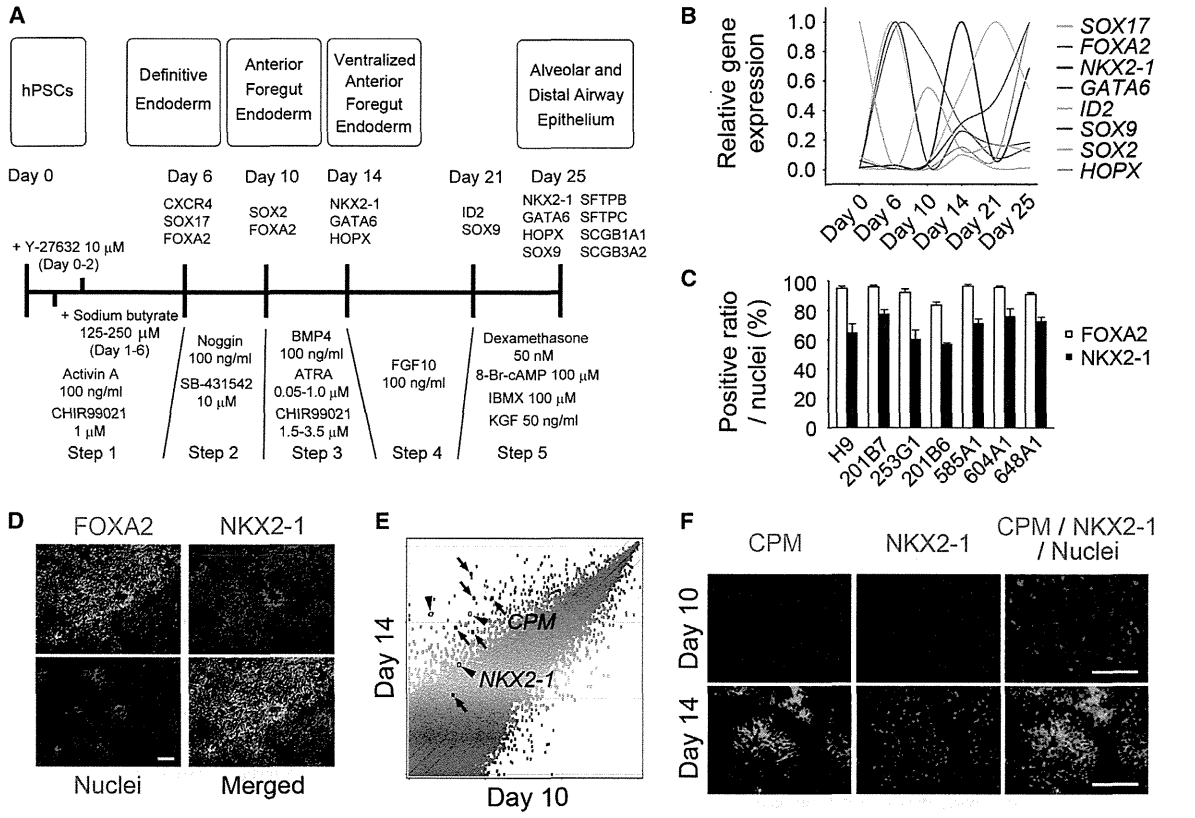

(legend on next page)

two copies of the *SFTPC* gene loci, in contrast to the A17-13 clone, in which random transgenic integration is supposed to have occurred, as indicated by three copies of the loci (Figure 3D). No copy-number variation was detected for the B2-3 clone, whereas a copy-number loss at chromosome 16 q23.3 and gain at chromosome 20 p13 were detected for the A17-14 clone (data not shown). Both *SFTPC-GFP* reporter hPSCs were then differentiated to the end of step 5 and GFP$^+$ and GFP$^-$ cells were obtained by FACS after the CPM$^+$ cells were sorted using MACS (Figure 3E). We confirmed the correlation between *GFP* and *SFTPC* on RT-PCR (Figure 3F). GFP was detected in SFTPC$^+$, SFTPB$^+$, and NKX2-1$^+$ cells for both clones (Figure 3G).

Alveolar Differentiation from CPM$^+$ VAFECs in 3D Coculture

We attempted 2D differentiation, reseeding the CPM$^+$ *SFTPC-GFP* reporter hPSCs purified from VAFECs on day 14 onto Matrigel-coated, 96-well plates. After 14 days of differentiation in step 5 medium, SFTPB became positive in the reseeded CPM$^+$ cells (Figure S2E); however, *SFTPC* was almost negative (Figure S4D, condition b). We obtained similar results when we sorted and reseeded CPM$^+$ cells on day 23 (Figure S2F). The discrepancy between the expression of SFTPB and SFTPC in developing human lungs was previously reported (Khoor et al., 1994). Therefore, we hypothesized that some missing factors are important for the coexpression of SFTPB and SFTPC. We then adopted a 3D coculture with fetal human lung fibroblasts (FHLFs) obtained at 17.5 weeks of gestation (Figure 4A). CPM$^+$ cells purified from VAFECs on day 14 and FHLFs were mixed at a ratio of 1:50 and reseeded onto cell inserts. After 10 days of differentiation in step 5 medium, GFP became positive in some spheroids (Figure 4B). The spheroids were subsequently examined with a transmission electron microscope and lamellar-body-like structures were noted (Figure 4C). On hematoxylin-and-eosin staining, cyst-like spheroids consisting of pseudostratified, columnar, or cuboidal cells with dark pink cytoplasm were observed in the CPM$^+$ cell-derived spheroids, whereas small pieces of spheroids consisting of cuboidal cells with clear cytoplasm were noted in the CPM$^-$ cell-derived spheroids (Figure S4A). On IF staining, CPM and NKX2-1 were double positive in most CPM$^+$ cell-derived spheroids, while GFP and SFTPC were double positive in some spheroids (Figure 4D). In the CPM$^-$ cell-derived spheroids, EPCAM was positive, whereas no CPM$^+$ or NKX2-1$^+$ cells were identified (Figure S4B). SFTPA, SFTPB, SFTPC, and SFTPD (representative markers of type II AECs) were positive in the CPM$^+$ cell-derived spheroids (Figure S4C). AQP5$^+$ cells were adjacent to SFTPC$^+$ cells in some spheroids (Figure 4D). ID2 and SOX9 (markers of differentiation into the distal lung-lineage fate) were positive in some NKX2-1$^+$ and CPM$^+$ cells, respectively (Figure S4C). Next, we trypsinized the cells in 3D structures and determined the proportion of SFTPC-GFP$^+$ cells, detecting 3.82% ± 0.50% cells obtained from the CPM$^+$ cell-derived 3D structures and 0.29% ± 0.03% cells obtained from the CPM$^-$ cell-derived structures including fibroblasts (Figure 4E). Excluding the fibroblasts, the ratio of the number of SFTPC-GFP$^+$ cells to that of EPCAM$^+$ cells was calculated to be 9.81% ± 1.81% in the CPM$^+$ cell-derived spheroids and 1.07% ± 0.16% in the CPM$^-$ cell-derived spheroids. Almost all of the GFP$^+$ cells sorted by FACS were SFTPC$^+$, whereas the GFP$^-$ cells were SFTPC$^-$ (Figure 4F). The levels of alveolar markers (*SFTPB* and *SFTPC*), rather than club cell markers (*SCGB1A1* and *SCGB3A2*), were significantly elevated following the 3D coculture differentiation of CPM$^+$ cells derived from three hPSC lines (H9 hESCs and parental 201B7 and 604A1 hiPSCs) compared with the 2D differentiation employing the three protocols separately starting on day 14 (Figure 1A; Green et al., 2011; Longmire et al., 2012) and the 3D coculture differentiation of CPM$^-$ cells (Figure 4G). Interestingly, the levels of *SFTPB* and *SFTPC* were quite low for 585A1 hiPSCs, suggesting

Figure 1. Identification of CPM as a Candidate Marker of NKX2-1$^+$ VAFECs

(A) Stepwise differentiation to AECs from hPSCs.

(B) Gene-expression levels of transcription factors from day 0 to day 25 (n = 3). Each value was normalized to the level of *β-ACTIN*. The relative expression level was scored with the maximum value set to 1.0.

(C) Induction efficiency of VAFECs analyzed by scoring the number of FOXA2$^+$ and NKX2-1$^+$ cells relative to the total number of nuclei in an average of ten randomly selected images (n = 3).

(D) FOXA2$^+$NKX2-1$^+$ VAFECs derived from 201B7 hiPSCs.

(E) Scatterplots comparing the global gene-expression profiles of AFECs (day 10) and VAFECs (day 14). *CPM* (arrows) and *NKX2-1* (arrowheads) are noted. The lines beside the diagonal line indicate a 2-fold cutoff change between the AFECs and VAFECs.

(F) Simultaneous increases of CPM and NKX2-1 detected by IF staining of AFECs (day 10) and VAFECs (day 14).

(G) CPM detected in NKX2-1$^+$, SOX9$^+$, SFTPB$^+$, SFTPC$^+$, and SCGB3A2$^+$ cells, but not in KRT5$^+$ cells, on day 25.

(H) CPM detected in NKX2-1$^+$ lung epithelial cells in fetal human lung.

(I) CPM in E12.5, E15.5, and E17.5 murine lungs.

Error bars show SEM. Scale bars, 100 μm. See also Figure S1 and Tables S1 and S2.

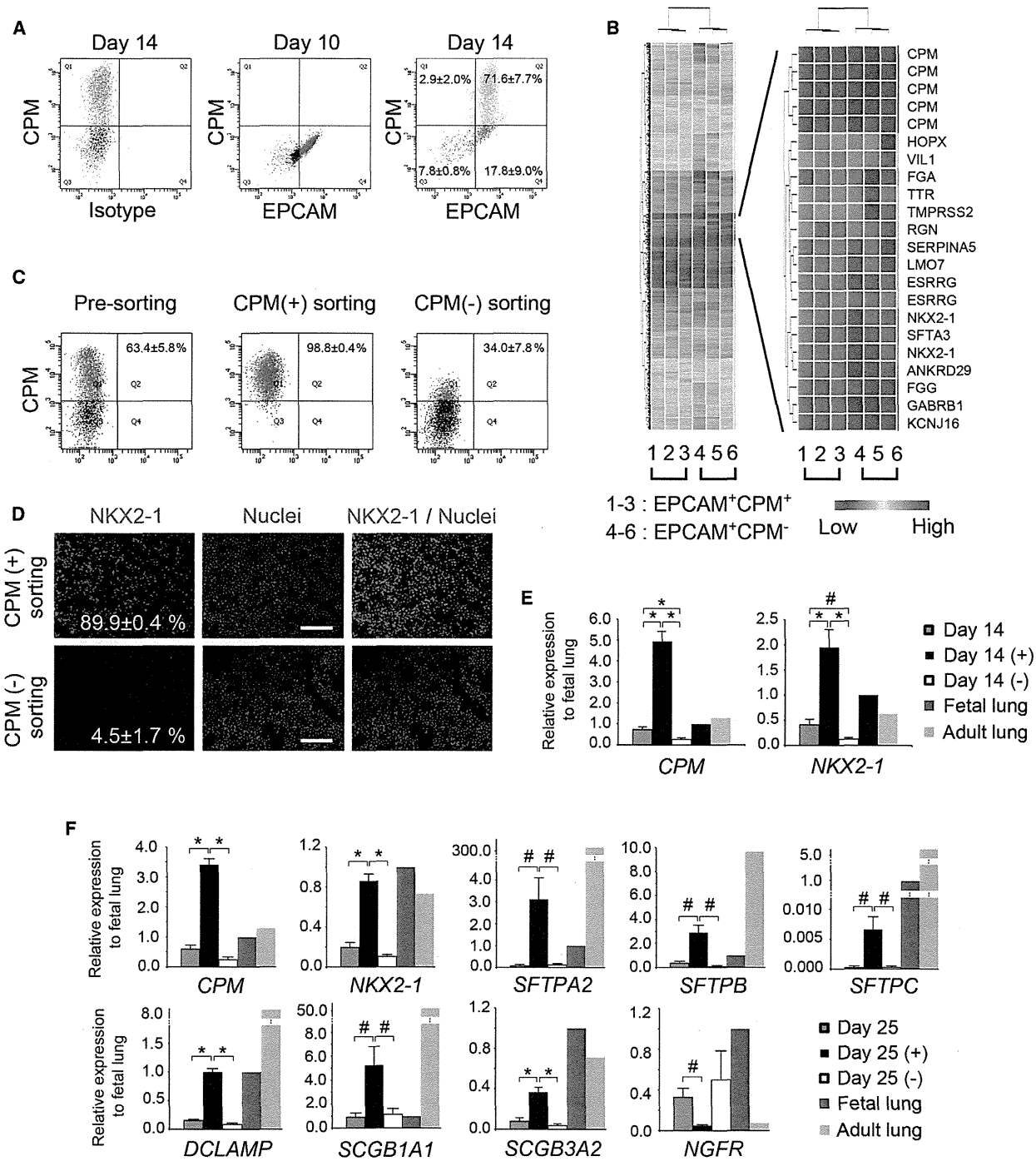

Figure 2. Isolation of CPM$^+$ VAFECs Using Anti-CPM Antibody

(A) Flow cytometry of VAFECs. EPCAM$^+$CPM$^+$ (Q2) and EPCAM$^+$CPM$^-$ cells (Q4) were isolated on day 14 (n = 3).

(B) Hierarchical clustering heatmaps of 336 genes with differences of >2-fold (FDR-adjusted $p < 0.05$) comparing EPCAM$^+$CPM$^+$ cells with EPCAM$^+$CPM$^-$ cells. The cluster of genes increased as the greatest fold change was magnified.

(C) Flow cytometry of MACS-sorted CPM$^+$ and CPM$^-$ cells from VAFECs (n = 3).

(D) NKX2-1$^+$ cells in FACS-sorted CPM$^+$ and CPM$^-$ cells derived from VAFECs analyzed by scoring the number of NKX2-1$^+$ cells relative to the total number of nuclei in an average of five randomly selected images (n = 3).

(legend continued on next page)

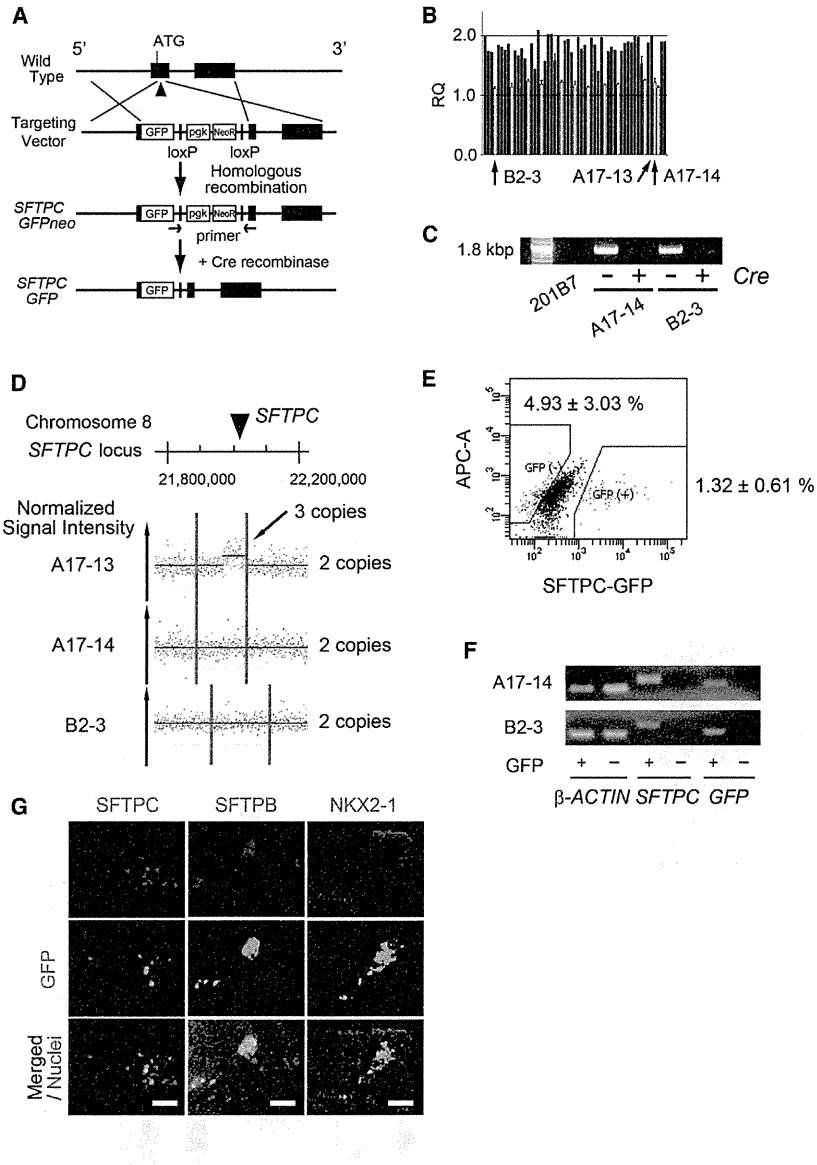

Figure 3. Generation of *SFTPC-GFP* Knockin hPSC Lines

(A) Strategy for BAC-based gene targeting to produce *SFTPC-GFP* knockin hPSC lines.

(B) Screening of knockin hPSC lines using TaqMan qPCR. Positive clones with candidate heterozygous deletion of the endogenous *SFTPC* gene are shown in white bars. Only clones that were initially suspected to be positive were tested independently three times.

(C) Genomic PCR to confirm the removal of the *pgk-NeoR* cassette by Cre-recombinase in the A17-14 and B2-3 *SFTPC-GFP* reporter hPSCs.

(D) SNP array analysis of the *SFTPC-GFP* knockin hPSC lines. The copy number of *SFTPC* gene loci was analyzed in A17-13, A17-14, and B2-3 clones. The A17-14 and B2-3 clones have two copies of the *SFTPC* gene loci, whereas the A17-13 clone has three copies of the loci. The red dots and y axis represent the normalized signal intensity of each SNP.

(E) Isolation of SFTPC$^-$GFP$^+$ and GFP$^-$ cells via FACS after sorting CPM$^+$ cells via MACS on day 25.

(F) RT-PCR analyses of GFP$^+$ and GFP$^-$ sorted cells in the A17-14 and B2-3 *SFTPC-GFP* reporter hPSC lines.

(G) Representative images of GFP detected in SFTPC$^+$, SFTPB$^+$, and NKX2-1$^+$ cells.

Error bars show SEM. Scale bars, 100 μm. See also Figure S3 and Tables S1 and S2.

that the concentration of retinoic acid required to induce NKX2-1$^+$ VAFECs in step 3 is less important for subsequent differentiation into AECs than the difference in the cell lines or donors. Moreover, the expression of *SFTPB* and *SFTPC* was small for the 2D and 3D differentiation of CPM$^+$ cells alone or FHLFs alone (Figure S4D). Finally, other cell-type markers (*AQP5* [type I AECs], *FOXJ1* [ciliated cells], and *AGR2* [goblet cells]) appeared to be elevated in the CPM$^+$ cell-derived structures rather than in the CPM$^-$ cell-derived structures, suggesting that cell-type markers other than club-cell markers were expressed in the CPM$^+$ cell-derived spheroids. *KRT5* (a basal cell marker, possibly including both airway and esophageal basal cells) was exclusively expressed in the CPM$^-$

(E) Levels of *CPM* and *NKX2-1* on day 14 before and after MACS-based purification of CPM$^+$ cells on qRT-PCR (n = 5).

(F) Levels of AEC and club-cell markers and *NGFR*, a proximal airway stem cell marker, on day 25 before and after MACS-based purification of CPM$^+$ cells (n = 5).

The gene-expression level observed in the fetal lungs was set at one. Values are presented as the mean ± SEM. Error bars show SEM. #p < 0.05, *p < 0.01. Scale bars, 100 μm. See also Figure S2 and Tables S1 and S2.

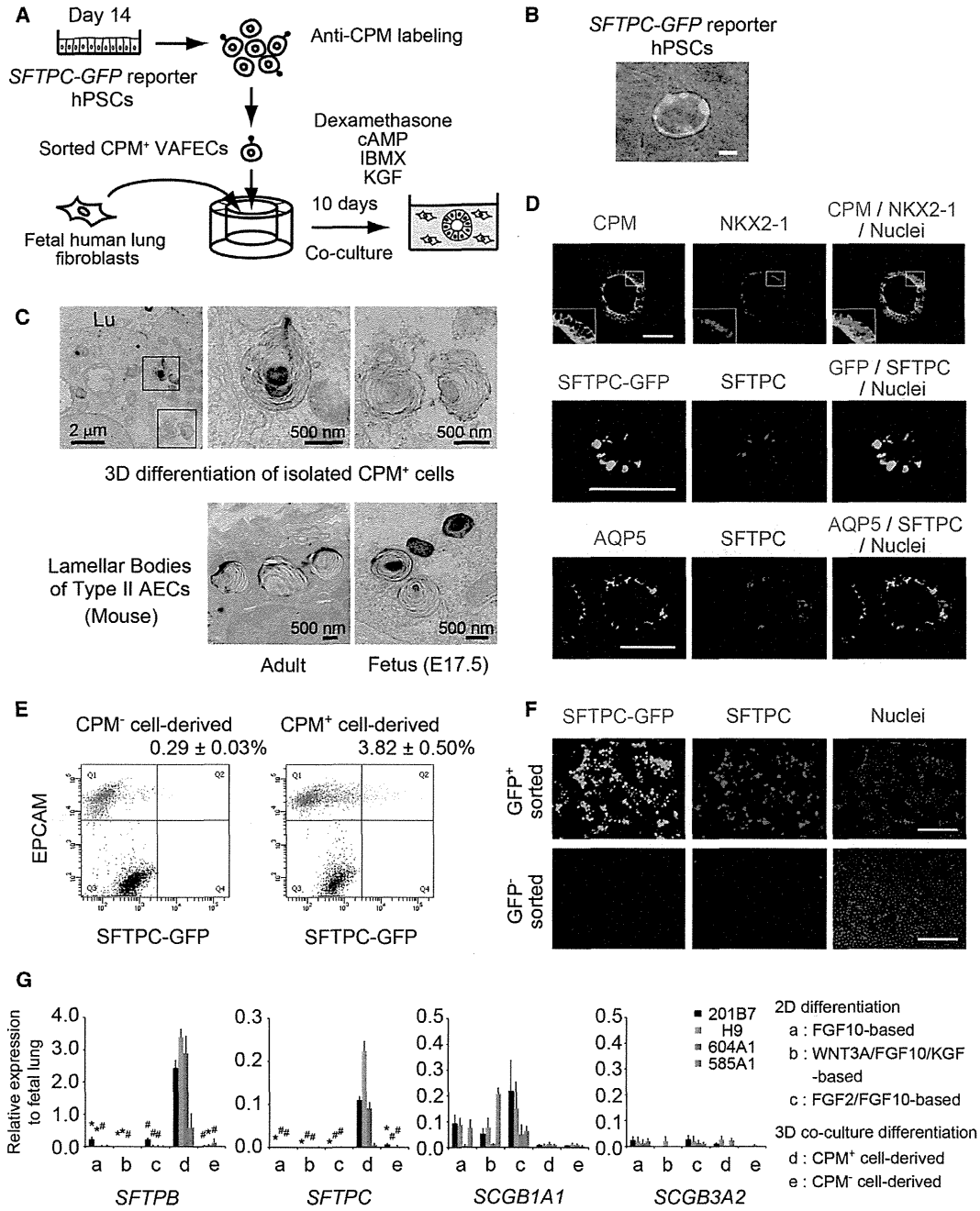

Figure 4. Alveolar Differentiation from CPM$^+$ VAFECs in 3D Coculture

(A) Strategy for inducing AECs via 3D coculture with FHLFs.

(B) SFTPC-GFP$^+$ cells detected in spheroids derived from isolated CPM$^+$ VAFECs.

(C) Transmission electron microscopy of lamellar-body-like structures observed in 3D coculture differentiation of CPM$^+$ cells compared with those observed in the adult and fetal murine lungs. Lu, lumen.

(D) IF staining of spheroids derived from CPM$^+$ VAFECs.

(E) Flow cytometry of SFTPC-GFP$^+$ cells in 3D coculture differentiation of CPM$^+$ cells or CPM$^-$ cells (n = 3).

(F) GFP$^+$ and GFP$^-$ cells isolated via FACS, spun down onto slides, and stained by anti-GFP and anti-SFTPC antibodies.

(legend continued on next page)

cell-derived structures. In addition, *PAX8* (a thyroid marker), *PAX6* (a neuron marker), and the other foregut endodermal lineage cells (*FOXN1*, *ALB*, and *PDX1*) were only minimally or slightly induced following 3D coculture differentiation (Figure S4E).

DISCUSSION

In this work, we identified CPM as a surface marker that is expressed in NKX2-1$^+$ VAFECs, including AEPCs, and demonstrated that the CPM$^+$ cell-derived spheroids obtained via 3D coculture differentiation with FHLFs enabled more efficient differentiation to AECs than did 2D differentiation. The gene-expression pattern of *CPM* in developing lungs has not received significant attention, although in situ hybridization of *Cpm* in anterior DECs as early as E7.5 in mice has been reported (Tamplin et al., 2008). Our data from IF staining of murine fetal lungs (Figure S1I) also suggest that lineage-tracing studies may provide answers to the following questions: Is Cpm a possible "specific" marker of lung-lineage progenitor cells such as Shh (Harris et al., 2006), Id2 (Rawlins et al., 2009a), and Nkx2-1 (Longmire et al., 2012)? What is the relationship between CPM$^+$ cells and bipotent cells that are capable of generating type I and type II AECs (Desai et al., 2014)? Do CPM$^+$ cells differentiate into type II AECs directly or indirectly via SFTPC$^+$SCGB1A1$^+$ cells (Kim et al., 2005; Rawlins et al., 2009b)? Furthermore, the present study suggests that a 3D microenvironment and coculture with FHLFs are important factors in the differentiation of progenitor cells into AECs rather than club cells. Although maintaining type II AECs in 2D conditions is often difficult (Dobbs, 1990; Yu et al., 2007), 3D conditions have recently been applied with better outcomes (Yu et al., 2007; McQualter et al., 2010; Barkauskas et al., 2013). Therefore, our 3D differentiation protocol appears to be a reasonable approach for maintaining differentiated type II AECs, although methods for expanding such cells for longer periods should be established in the next step.

The limitations of the present study include the fact that we were unable to demonstrate whether CPM is a more appropriate marker for lung-lineage cells than NKX2-1. Future studies focusing on the possible contribution of NKX2-1$^-$CPM$^+$ cells and/or NKX2-1$^+$CPM$^-$ cells to the differentiation of lung epithelial cells may resolve this issue, although we found only two isolatable populations of NKX2-1$^+$CPM$^+$ and NKX2-1$^-$CPM$^-$ cells using the present protocol. In addition, we were unable to demonstrate the highest induction efficiency of AECs, as recently described (Ghaedi et al., 2013), although we employed a different method for evaluating efficiency using *SFTPC-GFP* reporter hPSCs. Another limitation is that the functions of the induced AECs remain to be elucidated.

Nevertheless, the methods applied in the present study to induce and isolate AEPCs using CPM and consequently generate alveolar epithelial spheroids in a stepwise fashion may help to elucidate the complicated differentiation of human AECs and open the door for the development of new strategies for in vitro toxicology and cell replacement therapy, as well as screening for therapeutic drug compounds, in the future.

EXPERIMENTAL PROCEDURES

2D Differentiation

CHIR99021 (Axon Medchem), an activator of canonical Wnt signaling, was substituted for WNT3A (Mae et al., 2013). For details regarding the protocols used for each differentiation medium, see the Supplemental Experimental Procedures.

3D Differentiation

The protocol for the 3D culture was modified from a previous report (Barkauskas et al., 2013). For further details, see the Supplemental Experimental Procedures.

Ethics

The use of H9 hESCs was approved by the Ministry of Education, Culture, Sports, Science and Technology (MEXT) of Japan. Human ethics approval was obtained from the Institutional Review Board and Ethics Committee of Kyoto University Graduate School and Faculty of Medicine. Animal ethics approval was obtained from the Animal Ethics and Research Committee of Kyoto University.

Statistical Analysis

Values are expressed as the mean ± SEM and "n" stands for the number of independent experiments. Two-tailed Student's t test was performed to identify significant differences between two conditions of qRT-PCR.

ACCESSION NUMBERS

The NCBI GEO accession number for the microarray data reported in this paper is GSE53513.

(G) qRT-PCR comparing the 2D and 3D differentiation into AECs in H9 hESCs and 201B7 (parental), 604A1, and 585A1 hiPSCs. Each value of the gene expression was normalized to the level of *β-ACTIN*. The levels of the fetal lungs were set at one.
Values are presented as the mean ± SEM. Error bars show SEM. #$p < 0.05$, *$p < 0.01$. Scale bars, 100 μm unless otherwise indicated. See also Figure S4 and Tables S1 and S2.

SUPPLEMENTAL INFORMATION

Supplemental Information includes Supplemental Experimental Procedures, four figures, and two tables and can be found with this article online at http://dx.doi.org/10.1016/j.stemcr.2014.07.005.

AUTHOR CONTRIBUTIONS

S.G., I.I., and K.O. designed the study. S.G., T.N., Y.Y., S.K., Y.K., and A.S.-O. performed the experiments. S.G., I.I., T.N., Y.Y., S.K., A.S.-O., S.O., and K.O. analyzed the data. S.G. and I.I. wrote the manuscript through fruitful discussions with and supervision by H.M., S.M., T.H., S.O., K.O., and M.M. M.F., S.-I.M., T.T., and K.O. provided the method for inducing definitive endoderm and advised on the methods used for vector construction and other basic techniques.

ACKNOWLEDGMENTS

We are grateful to K. Okita, K. Takahashi, T. Aoi, M. Kajiwara, I. Asaka, and S. Yamanaka (Center for iPS Cell Research and Application, Kyoto University) for providing cell lines, plasmids, the method of iPSC culture, and endoderm differentiation. We thank K. Okamoto-Furuta and H. Kohda (Division of Electron Microscopic Study, Center for Anatomical Studies, Kyoto University) for technical assistance with the electron microscope. We also thank S. Tsukita and A. Tamura (Osaka University) for advice on electron microscopy, S. Kimura (National Cancer Institute, NIH) for providing the anti-SCGB3A2 antibody, Y. Ito for excellent advice and assistance, and Y. Maeda and A. Inazumi for technical assistance. Fluorescence studies and gene-expression microarray analyses were performed in part at the Medical Research Support Center of Kyoto University. This work was supported by Grants-in-Aid for Scientific Research (KAKENHI 22249031 and 23591146) from MEXT of Japan.

Received: January 17, 2014
Revised: July 18, 2014
Accepted: July 18, 2014
Published: August 21, 2014

REFERENCES

Barkauskas, C.E., Cronce, M.J., Rackley, C.R., Bowie, E.J., Keene, D.R., Stripp, B.R., Randell, S.H., Noble, P.W., and Hogan, B.L. (2013). Type 2 alveolar cells are stem cells in adult lung. J. Clin. Invest. *123*, 3025–3036.

Desai, T.J., Brownfield, D.G., and Krasnow, M.A. (2014). Alveolar progenitor and stem cells in lung development, renewal and cancer. Nature *507*, 190–194.

Dobbs, L.G. (1990). Isolation and culture of alveolar type II cells. Am. J. Physiol. *258*, L134–L147.

Firth, A.L., Dargitz, C.T., Qualls, S.J., Menon, T., Wright, R., Singer, O., Gage, F.H., Khanna, A., and Verma, I.M. (2014). Generation of multiciliated cells in functional airway epithelia from human induced pluripotent stem cells. Proc. Natl. Acad. Sci. USA *111*, E1723–E1730.

Ghaedi, M., Calle, E.A., Mendez, J.J., Gard, A.L., Balestrini, J., Booth, A., Bove, P.F., Gui, L., White, E.S., and Niklason, L.E. (2013). Human iPS cell-derived alveolar epithelium repopulates lung extracellular matrix. J. Clin. Invest. *123*, 4950–4962.

Gonzales, L.W., Guttentag, S.H., Wade, K.C., Postle, A.D., and Ballard, P.L. (2002). Differentiation of human pulmonary type II cells in vitro by glucocorticoid plus cAMP. Am. J. Physiol. Lung Cell. Mol. Physiol. *283*, L940–L951.

Green, M.D., Chen, A., Nostro, M.C., d'Souza, S.L., Schaniel, C., Lemischka, I.R., Gouon-Evans, V., Keller, G., and Snoeck, H.W. (2011). Generation of anterior foregut endoderm from human embryonic and induced pluripotent stem cells. Nat. Biotechnol. *29*, 267–272.

Harris, K.S., Zhang, Z., McManus, M.T., Harfe, B.D., and Sun, X. (2006). Dicer function is essential for lung epithelium morphogenesis. Proc. Natl. Acad. Sci. USA *103*, 2208–2213.

Huang, S.X., Islam, M.N., O'Neill, J., Hu, Z., Yang, Y.G., Chen, Y.W., Mumau, M., Green, M.D., Vunjak-Novakovic, G., Bhattacharya, J., and Snoeck, H.W. (2014). Efficient generation of lung and airway epithelial cells from human pluripotent stem cells. Nat. Biotechnol. *32*, 84–91.

Kajiwara, M., Aoi, T., Okita, K., Takahashi, R., Inoue, H., Takayama, N., Endo, H., Eto, K., Toguchida, J., Uemoto, S., and Yamanaka, S. (2012). Donor-dependent variations in hepatic differentiation from human-induced pluripotent stem cells. Proc. Natl. Acad. Sci. USA *109*, 12538–12543.

Khoor, A., Stahlman, M.T., Gray, M.E., and Whitsett, J.A. (1994). Temporal-spatial distribution of SP-B and SP-C proteins and mRNAs in developing respiratory epithelium of human lung. J. Histochem. Cytochem. *42*, 1187–1199.

Kim, C.F., Jackson, E.L., Woolfenden, A.E., Lawrence, S., Babar, I., Vogel, S., Crowley, D., Bronson, R.T., and Jacks, T. (2005). Identification of bronchioalveolar stem cells in normal lung and lung cancer. Cell *121*, 823–835.

Kimura, S., Hara, Y., Pineau, T., Fernandez-Salguero, P., Fox, C.H., Ward, J.M., and Gonzalez, F.J. (1996). The T/ebp null mouse: thyroid-specific enhancer-binding protein is essential for the organogenesis of the thyroid, lung, ventral forebrain, and pituitary. Genes Dev. *10*, 60–69.

Longmire, T.A., Ikonomou, L., Hawkins, F., Christodoulou, C., Cao, Y., Jean, J.C., Kwok, L.W., Mou, H., Rajagopal, J., Shen, S.S., et al. (2012). Efficient derivation of purified lung and thyroid progenitors from embryonic stem cells. Cell Stem Cell *10*, 398–411.

Mae, S., Shono, A., Shiota, F., Yasuno, T., Kajiwara, M., Gotoda-Nishimura, N., Arai, S., Sato-Otubo, A., Toyoda, T., Takahashi, K., et al. (2013). Monitoring and robust induction of nephrogenic intermediate mesoderm from human pluripotent stem cells. Nat. Commun. *4*, 1367.

McQualter, J.L., Yuen, K., Williams, B., and Bertoncello, I. (2010). Evidence of an epithelial stem/progenitor cell hierarchy in the adult mouse lung. Proc. Natl. Acad. Sci. USA *107*, 1414–1419.

Mou, H., Zhao, R., Sherwood, R.I., Ahfeldt, T., Lapey, A., Sicillian, L., Izvolsky, K.I., Musunuru, K., Cowan, C., and Rajagopal, J. (2012). Generation of multipotent embryonic lung and airway

progenitors from mouse ESCs and patient-specific cystic fibrosis iPSCs. Cell Stem Cell *10*, 385–397.

Nagae, A., Abe, M., Becker, R.P., Deddish, P.A., Skidgel, R.A., and Erdös, E.G. (1993). High concentration of carboxypeptidase M in lungs: presence of the enzyme in alveolar type I cells. Am. J. Respir. Cell Mol. Biol. *9*, 221–229.

Nakagawa, M., Koyanagi, M., Tanabe, K., Takahashi, K., Ichisaka, T., Aoi, T., Okita, K., Mochiduki, Y., Takizawa, N., and Yamanaka, S. (2008). Generation of induced pluripotent stem cells without Myc from mouse and human fibroblasts. Nat. Biotechnol. *26*, 101–106.

Okita, K., Yamakawa, T., Matsumura, Y., Sato, Y., Amano, N., Watanabe, A., Goshima, N., and Yamanaka, S. (2013). An efficient nonviral method to generate integration-free human-induced pluripotent stem cells from cord blood and peripheral blood cells. Stem Cells *31*, 458–466.

Rawlins, E.L., Clark, C.P., Xue, Y., and Hogan, B.L. (2009a). The Id2+ distal tip lung epithelium contains individual multipotent embryonic progenitor cells. Development *136*, 3741–3745.

Rawlins, E.L., Okubo, T., Xue, Y., Brass, D.M., Auten, R.L., Hasegawa, H., Wang, F., and Hogan, B.L. (2009b). The role of Scgb1a1+ Clara cells in the long-term maintenance and repair of lung airway, but not alveolar, epithelium. Cell Stem Cell *4*, 525–534.

Rock, J.R., and Hogan, B.L. (2011). Epithelial progenitor cells in lung development, maintenance, repair, and disease. Annu. Rev. Cell Dev. Biol. *27*, 493–512.

Rock, J.R., Onaitis, M.W., Rawlins, E.L., Lu, Y., Clark, C.P., Xue, Y., Randell, S.H., and Hogan, B.L. (2009). Basal cells as stem cells of the mouse trachea and human airway epithelium. Proc. Natl. Acad. Sci. USA *106*, 12771–12775.

Takahashi, K., Tanabe, K., Ohnuki, M., Narita, M., Ichisaka, T., Tomoda, K., and Yamanaka, S. (2007). Induction of pluripotent stem cells from adult human fibroblasts by defined factors. Cell *131*, 861–872.

Tamplin, O.J., Kinzel, D., Cox, B.J., Bell, C.E., Rossant, J., and Lickert, H. (2008). Microarray analysis of Foxa2 mutant mouse embryos reveals novel gene expression and inductive roles for the gastrula organizer and its derivatives. BMC Genomics *9*, 511.

Thomson, J.A., Itskovitz-Eldor, J., Shapiro, S.S., Waknitz, M.A., Swiergiel, J.J., Marshall, V.S., and Jones, J.M. (1998). Embryonic stem cell lines derived from human blastocysts. Science *282*, 1145–1147.

Whitsett, J.A., Wert, S.E., and Weaver, T.E. (2010). Alveolar surfactant homeostasis and the pathogenesis of pulmonary disease. Annu. Rev. Med. *61*, 105–119.

Wong, A.P., Bear, C.E., Chin, S., Pasceri, P., Thompson, T.O., Huan, L.J., Ratjen, F., Ellis, J., and Rossant, J. (2012). Directed differentiation of human pluripotent stem cells into mature airway epithelia expressing functional CFTR protein. Nat. Biotechnol. *30*, 876–882.

Yu, W., Fang, X., Ewald, A., Wong, K., Hunt, C.A., Werb, Z., Matthay, M.A., and Mostov, K. (2007). Formation of cysts by alveolar type II cells in three-dimensional culture reveals a novel mechanism for epithelial morphogenesis. Mol. Biol. Cell *18*, 1693–1700.

Stem Cell Research (2015) 14, 185–197

Available online at www.sciencedirect.com

ScienceDirect

www.elsevier.com/locate/scr

Cell aggregation optimizes the differentiation of human ESCs and iPSCs into pancreatic bud-like progenitor cells

Taro Toyoda[a], Shin-Ichi Mae[a], Hiromi Tanaka[a], Yasushi Kondo[a,b], Michinori Funato[a,c], Yoshiya Hosokawa[a,d], Tomomi Sudo[a], Yoshiya Kawaguchi[a], Kenji Osafune[a,*]

[a] *Center for iPS Cell Research and Application (CiRA), Kyoto University, 53 Kawahara-cho, Shogoin, Sakyo-ku, Kyoto 606-8507, Japan*
[b] *Department of Diabetes and Clinical Nutrition, Graduate School of Medicine, Kyoto University, 54 Kawahara-cho, Shogoin, Sakyo-ku, Kyoto 606-8507, Japan*
[c] *Department of Clinical Research, National Hospital Organization, Nagara Medical Center, 1300-7 Nagara, Gifu 502-0071, Japan*
[d] *Department of Metabolic Medicine, Osaka University Graduate School of Medicine, 2-2 Yamadaoka, Suita 565-0871, Japan*

Received 15 August 2014; received in revised form 28 December 2014; accepted 19 January 2015

Abstract Embryonic pancreatic bud cells, the earliest pancreas-committed cells, generated from human embryonic stem cells (hESCs) and induced pluripotent stem cells (hiPSCs) have been shown to differentiate into mature pancreatic β-cells *in vivo*, indicating the feasibility of hESC/iPSC-based cell therapy for diabetes. However, the key factors required for the differentiation of these cells into pancreatic bud cells are incompletely understood. The purpose of this study was to establish culture conditions that efficiently induce PDX1$^+$NKX6.1$^+$ pancreatic bud cells from hESCs/iPSCs. We differentiated a hESC line, KhES-3, into pancreatic lineages with a stepwise protocol recapitulating developmental process. The induction rate of PDX1$^+$NKX6.1$^+$ cells was correlated with cell density in adherent cultures, and markedly improved with cell aggregation cultures. The positive effects of cell aggregation cultures on the differentiation of pancreatic bud cells were reproduced in multiple hESC/iPSC lines. The human PDX1$^+$NKX6.1$^+$ cells developed into pancreatic epithelia after implantation into immunocompromised mice. Moreover, human C-peptide secretion into mouse bloodstream was stimulated by glucose challenges after *in vivo* maturation. Taken together, these results suggest that cultures with high cell density are crucial for the differentiation of pancreas-committed progenitor cells from hESCs/iPSCs. Our findings may be applicable for the development of hESC/iPSC-based cell therapy for diabetes.

Introduction

Diabetes is caused by an absolute or relative insufficiency of insulin which is secreted from pancreatic β-cells, resulting in impaired glucose metabolism in the entire body (Mathis and

* Corresponding author. Fax: +81 75 366 7077.
E-mail address: osafu@cira.kyoto-u.ac.jp (K. Osafune).

http://dx.doi.org/10.1016/j.scr.2015.01.007
1873-5061/

Vence, 2001; Donath and Halban, 2004). The supplementation of β-cell function is an effective therapeutic strategy, but the insufficient cell supply is a major obstacle to this intervention (Matsumoto, 2011). Therefore, vigorous efforts have been made to develop a stable source of pancreatic cells for clinical use.

Human embryonic stem cells (hESCs) and induced pluripotent stem cells (hiPSCs) are attractive cell sources due to their potential for unlimited proliferation and differentiation (Dominguez-Bendala et al., 2011; McCall et al., 2010). Indeed, a number of groups have generated immature pancreatic β cell-like cells, which are referred to as insulin-producing or insulin-secreting cells, from hESCs/iPSCs *in vitro* (D'Amour et al., 2006; Jiang et al., 2007a,b; Zhang et al., 2009; Nostro et al., 2011; Kroon et al., 2008; Mfopou et al., 2010; Shim et al., 2007; Cai et al., 2010; Kelly et al., 2011; Xu et al., 2011; Kunisada et al., 2012; Rezania et al., 2011, 2012, 2013; Schulz et al., 2012; Bruin et al., 2013; Sui et al., 2013). Despite the difficulties in generating genuine β-cells *in vitro*, mature insulin-producing cells with the potential for glucose responsiveness have been obtained following the implantation of hESC-derived pancreatic progenitors into immunodeficient mice (D'Amour et al., 2006; Kroon et al., 2008; Shim et al., 2007; Kelly et al., 2011; Rezania et al., 2012, 2013; Bruin et al., 2013). Therefore, implantation of pancreatic progenitors, instead of β-cells, is also considered to be a therapeutic option for diabetes.

Previous reports have described the generation of pancreatic lineage cells, such as pancreatic progenitors and insulin-producing cells, from hESCs/iPSCs *in vitro*, using stepwise differentiation protocols that recapitulate pancreatic development (D'Amour et al., 2006; Jiang et al., 2007a,b; Zhang et al., 2009; Nostro et al., 2011; Kroon et al., 2008; Mfopou et al., 2010; Shim et al., 2007; Cai et al., 2010; Kelly et al., 2011; Xu et al., 2011; Kunisada et al., 2012; Rezania et al., 2011, 2012, 2013; Schulz et al., 2012; Bruin et al., 2013; Sui et al., 2013). However, the quantitative differences in the differentiation efficiency among hESC/iPSC lines make it difficult to obtain the stable production of pancreatic lineage cells with sufficient purity for use in the clinical setting (Osafune et al., 2008). One of the solutions for this is the establishment of stable differentiation methods that can be more broadly applied to multiple hESC/iPSC lines, based on a complete understanding of the mechanisms of pancreatic organogenesis.

The major components of the pancreas are exocrine, duct and endocrine cells, which originate from the endoderm layer of early embryos marked by the co-expression of transcription factors Sox17 and FoxA2 (Jennings et al., 2013). The endodermal layer extends and folds to form the primitive gut tube expressing Hnf1β and Hnf4α, which has potential to differentiate into respiratory apparatus, digestive tract and endocrine organs, including the pancreas. Distinct pancreatic organogenesis morphologically starts at the posterior foregut area in the primitive gut tube following the expression of a transcription factor, Pdx1 (Jorgensen et al., 2007; Jensen, 2004). Two parts of the Pdx1$^+$ gut tube thicken to form the dorsal and ventral pancreatic buds. It should be noted that the early pancreatic epithelia formed by the stratification of the single cell layer of the gut tube and its protrusion into the surrounding mesenchyme exist as a three-dimensional highly-dense aggregate expressing additional transcription factors, Ptf1a and Nkx6.1, during the process of bud formation (Hald et al., 2008; Ahnfelt-Ronne et al., 2012; Kawaguchi et al., 2002; Villasenor et al., 2010). After that, microlumens appear and fuse to form epithelial structures with a branched tubular network within the aggregated pancreatic buds. Some epithelia differentiate into hormone-producing endocrine lineages, such as insulin-secreting β-cells and glucagon-secreting α-cells, and migrate into the mesenchyme to form pancreatic islets. Therefore, during the long process of islet formation, cells experience dynamic structural changes.

The Pdx1 expression is first detected at the presumptive bud area, maintained throughout the entire pancreatic development and eventually localized to β- and δ-cells (Jorgensen et al., 2007; Serup et al., 1995). However, the Pdx1 expression is not exclusive to the pancreas in gut tube, and extends anteriorly into the posterior stomach, duodenum and biliary system in the middle of embryogenesis (Jorgensen et al., 2007; Fukuda et al., 2006). On the other hand, the expression of Nkx6.1 and Ptf1a is found only in Pdx1$^+$ pancreatic buds and these are specific for pancreatic epithelium. Nkx6.1 and Ptf1a expression is eventually restricted to β- and exocrine acinar cells, respectively (Hald et al., 2008; Oster et al., 1998; Pan et al., 2013). Therefore, pancreatic bud cells co-expressing Pdx1, Ptf1a and Nkx6.1 are considered to be the earliest pancreas-committed progenitors. In fact, the results of implantation experiments have demonstrated that the PDX1$^+$NKX6.1$^+$ cells are progenitors that specifically differentiate into pancreatic cells (Kelly et al., 2011; Rezania et al., 2013).

In the current study, we evaluated the morphological characteristics of the pancreatic bud formation and tested the hypothesis that a high cell density is a key factor required to induce pancreatic bud cells in hESC/iPSC cultures. For this purpose, we compared the induction efficiency of the PDX1$^+$NKX6.1$^+$ cells in aggregation cultures with that in planar culture conditions, and performed the implantation of the PDX1$^+$NKX6.1$^+$ cells into immunocompromised mice to confirm whether the generated cells had the potential to differentiate into pancreatic lineages *in vivo*. We found that a high cell density is a crucial factor to induce PDX1$^+$NKX6.1$^+$ pancreatic bud cells *in vitro*, which can further differentiate into pancreatic epithelia and mature into functional endocrine cells *in vivo*. We also found that NKX6.1$^+$ cells originated from PDX1^{high} cells among heterogeneous PDX1$^+$ cell populations.

Material and methods

In vitro differentiation of hESCs/iPSCs

The maintenance culture of a hESC line, KhES-3 (Suemori et al., 2006), and five hiPSC lines; 585A1, 604B1, 692D2, 648B1 and 409B2 (Okita et al., 2011; Kajiwara et al., 2012) was performed as described previously (Mae et al., 2013). For feeder-free cultures, cells were maintained with Essential 8 medium (Thermo Fisher Scientific, Waltham, MA) according to the manufacturer's instructions. Experiments with hESCs/

iPSCs were approved by the ethics committee of the Department of Medicine and Graduate School of Medicine, Kyoto University. Cells were directed into key stages of pancreatic development, including definitive endoderm (Stage 1), primitive gut tube (Stage 2), posterior foregut (Stage 3) and pancreatic bud (Stage 4). The final protocol was as follows (Fig. 1A):

Stage 1 hESC/iPSC colonies grown on a feeder layer were first deprived of feeder cells and dissociated into

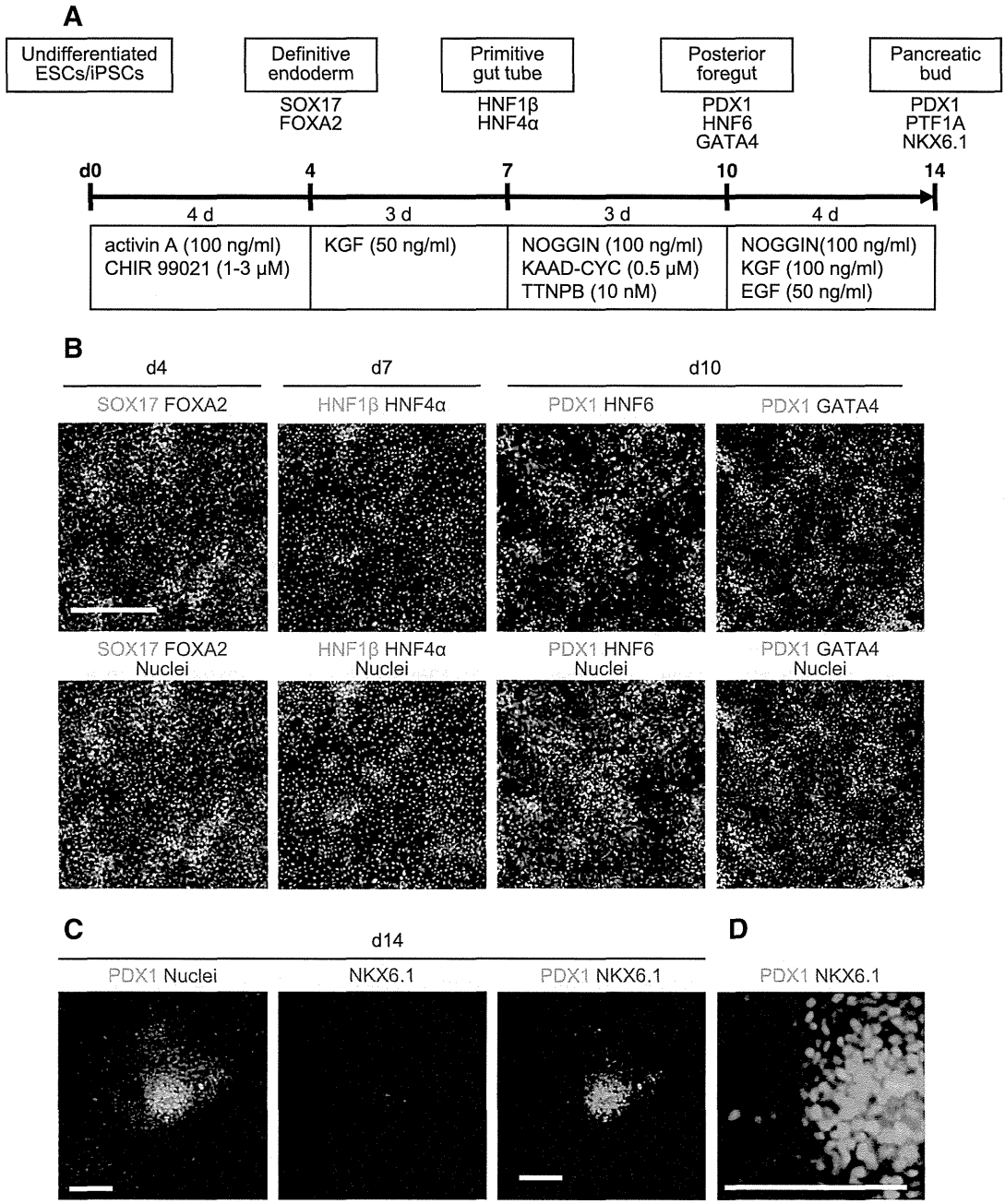

Figure 1 PDX1^{+}NKX6.1^{+} cells are localized at aggregated areas. (A) A schematic diagram of the procedures used for the differentiation of pancreatic bud cells from human ESCs. (B–D) A hESC line, KhES-3, was differentiated into definitive endoderm, primitive gut tube endoderm, posterior foregut and pancreatic bud, and was analyzed by immunostaining for representative markers. (D) A magnified image of (C). Note that only the aggregated areas of PDX1^{high} cells co-expressed NKX6.1. SOX17, SRY (sex determining region Y)-box17; FOXA2, forkhead box protein A2; HNF, hepatocyte nuclear factor; PDX1, pancreatic and duodenal homeobox 1; GATA4, GATA binding protein 4; NKX6.1, NK6 transcription factor related, locus 1. Scale bars, 300 μm in B and 100 μm in C and D.

single cells as described previously (Suemori et al., 2006). The cells were resuspended with Stage 1 medium containing RPMI 1640 medium (NACALAI TESQUE, Kyoto, Japan) supplemented with 2% (vol/vol) growth factor reduced B27 (GFR-B27, Thermo Fisher Scientific), 50 U/ml penicillin/streptomycin (P/S, Thermo Fisher Scientific), 100 ng/ml activin A (R&D Systems, Minneapolis, MN), 3 μM CHIR99021 (Axon Medchem, Groningen, Netherlands) and 10 μM Y-27632 (Wako, Osaka, Japan), seeded on Matrigel (Becton Dickinson, Franklin Lakes, NJ)-coated plates at a density of 1×10^5 cells/cm^2 and cultured for one day. For the next three days, the cells were cultured in RPMI 1640 medium with 2% GFR-B27, 50 U/ml P/S, 100 ng/ml activin A and 1 μM CHIR99021.

Stage 2 The cells were exposed to Improved MEM Zinc Option (iMEM) medium (Thermo Fisher Scientific) supplemented with 1% GFR-B27, 100 U/ml P/S (iMEM-B27) and 50 ng/ml keratinocyte growth factor (KGF; R&D Systems) for three days.

Stage 3 The cultures were continued for three days in iMEM-B27 with 0.5 μM 3-Keto-N-aminoethyl-N′-aminocaproyldihydrocinnamoyl cyclopamine (KAAD-CYC; Toronto Research Chemicals, Ontario, Canada), 0.5 nM 4-[(E)-2-(5,6,7,8-Tetrahydro-5,5,8,8-tetramethyl-2-naphthalenyl)-1-propenyl]-benzoic acid (TTNPB, Santa Cruz Biotechnology, Dallas, TX) and 100 ng/ml NOGGIN (Pepro-tech, Rocky Hill, NJ).

Stage 4 The cells were cultured for four to 20 days in iMEM-B27 with 100 ng/ml KGF, 100 ng/ml NOGGIN and 50 ng/ml epidermal growth factor (EGF, R&D Systems). For monolayer and aggregation cultures, the cells after Stage 3 treatments were dissociated into single cells by gentle pipetting after treatment with 0.25% trypsin–EDTA. The same inducing factors were used as described above, except for the addition of 10 μM Y-27632 to the Stage 4 treatments. For monolayer cultures, the cells were seeded on Matrigel-coated plates at a density of 6–48 × 10^4 cells/cm^2. To evaluate various extracellular matrices, the cells were seeded on laminin-111 (10 μg/ml; BioLamina, Sundbyberg, Sweden), fibronectin (5 μg/ml, Merck, Whitehouse Station, NJ), Synthemax (Corning, Corning, NY) and collagen I plates (Becton Dickinson). For aggregation cultures, the cells were seeded on a low-binding plate at a density of 3–30 × 10^3 cells/well.

Immunostaining

The cells were fixed with 4% paraformaldehyde (PFA) for 20 min at 4 °C. Then, immunostaining was performed as described previously (Mae et al., 2013). The primary antibodies used are detailed in Supplementary Table 1. The cell aggregates or implanted grafts were fixed with 4% PFA for one to two days at 4 °C. After washing with PBS, the samples were equilibrated in a 10–30% sucrose solution at room temperature for 1 h, and then mounted and frozen. The frozen blocks were sectioned at 10–30 μm, and immunostaining was performed after removing the mounting medium. For quantification of the Ki-67$^+$ and cleaved-Caspase3$^+$ cell ratios, immunostained cells were analyzed using an image analyzer CellInsight NXT (Thermo Fisher Scientific, Waltham, MA) or manual counting.

Flow cytometry

The cells were dissociated into single cells with 0.25% trypsin–EDTA treatment, fixed, permeabilized and blocked with a BD Cytofix/Cytoperm Kit (Becton Dickinson). Then, cells were stained with the antibodies detailed in Supplementary Table 1.

Quantitative real-time reverse transcription-polymerase chain reaction (qRT-PCR)

Total RNA was isolated from the cells with an RNeasy kit (Qiagen, Venlo, Netherlands), and cDNA was prepared with a ReverTra Ace qPCR RT Master Mix (TOYOBO, Osaka, Japan) and oligo (dT)20 primer, according to the manufacturer's instructions. The qRT-PCR analysis was carried out with SYBR Premix Ex Taq II (Takara, Otsu, Japan). The expression of each gene was normalized to the level of glyceraldehyde-3-phosphate dehydrogenase (GAPDH) expression. The primer sequences used are shown in Supplementary Table 2.

Animal studies and transplantation experiments

All animal experiments were performed in accordance with the Guidelines for Animal Experiments of Kyoto University. Male seven- to 14-week-old NOD.CB17-Prkdc^{scid}/J mice (NOD–SCID, Charles River Laboratories Japan, Yokohama, Japan) were maintained on a 12-h light/dark cycle with *ad libitum* access to a standard irradiated diet. Mice were anesthetized with inhalable isoflurane and received implants of hESC-derived cell aggregates after Stage 4. Stage 4 day 4 cell aggregates (30×10^3 cells/aggregate) were cultured in Stage 4 medium with or without an ALK5 inhibitor (Santa Cruz) for one to two additional days before implantation. Then, two hundred cell aggregates per mouse were implanted under a kidney subcapsule. At 30–210 days after implantation, the mice were sacrificed and the serial sections of grafts were examined by immunostaining, as described above.

The graft function was assessed by measuring human C-peptide levels in mouse plasma in response to glucose administration. The mice were fasted for >5 h, and a 30% glucose solution was administered by intraperitoneal injection at a dose of 3.0 g/kg body weight. Blood samples were collected prior to and at 30 min after the glucose administration *via* a tail vein into heparinized capillaries. The plasma human C-peptide level was analyzed by an ELISA (Mercodia, Uppsala, Sweden), according to the manufacturer's instructions. All metabolic analyses were performed in conscious and restrained animals.

Statistical analysis

The statistical analyses were performed using paired t-tests (SigmaStat 3.5, Systat, San Jose, CA). The differences between groups were considered significant for values of $p < 0.05$.

Results

hESC-derived PDX1$^+$NKX6.1$^+$ cells are formed at aggregated areas of adhesion cultures

To examine the differentiation of PDX1$^+$NKX6.1$^+$ pancreatic bud-like cells from a hESC line, KhES-3, we developed a directed differentiation protocol with a monolayer culture format by modifying the previously reported methods (Kunisada et al., 2012; Schulz et al., 2012) (Fig. 1A). As analyzed by immunostaining for representative markers for each step, we effectively obtained cells of the definitive endoderm (SOX17$^+$FOXA2$^+$), gut tube endoderm (HNF4α^+HNF1β^+) and posterior foregut (PDX1$^+$HNF6$^+$ or PDX1$^+$GATA4$^+$) (Fig. 1B).

Further differentiation of hESC-derived posterior foregut toward the pancreatic bud yielded only a small number of PDX1$^+$NKX6.1$^+$ cells. Most NKX6.1$^+$ cells were located in the aggregated areas composed of cells showing bright PDX1 fluorescent signals, whereas the PDX1$^+$NKX6.1$^-$ cells were mostly found in the remaining monolayered areas (Figs. 1C and D). The areas of PDX1$^+$NKX6.1$^+$ cells were expanded gradually around the aggregates (data not shown), thus indicating their further differentiation into PDX1$^+$NKX6.1$^+$ cells or the proliferation of PDX1$^+$NKX6.1$^+$ cells within the aggregates. Our observation of PDX1$^+$NKX6.1$^+$ cells in the aggregated areas of adhesion cultures was reminiscent of the pancreatic budding in mouse embryos (Jorgensen et al., 2007).

Aggregation cultures efficiently differentiate hESC-derived PDX1$^+$ foregut into PDX1$^+$NKX6.1$^+$ pancreatic buds

Next, to investigate whether cell aggregation itself is a factor to promote NKX6.1$^+$ cell differentiation, the PDX1$^+$ cells on culture day 10 were either treated with Stage 4 factors (S4F), or were dissociated and treated with Stage 4 factors in monolayer cultures at different cell densities (6–48 $\times$ 10^4 cells/cm^2) (S4F-2D) or in suspension cultures with cellular aggregates of different sizes (3–30 $\times$ 10^3 cells/aggregate) (S4F-AG) (Fig. 2A). On day 14, the S4F cells showed a mixture of aggregated and monolayered areas, while the cells treated with the S4F-2D formed monolayers without any aggregated areas (Fig. 2B). Before the induction on day 10, there were no PDX1$^+$NKX6.1$^+$ cells (Fig. 2C). The S4F cultures generated PDX1$^+$NKX6.1$^+$ cells at an 18 $\pm$ 5% induction rate. On the other hand, the induction rate of PDX1$^+$NKX6.1$^+$ cells was consistently lower (3–17%) in the S4F-2D cultures in a coating with various extracellular matrices (Fig. S1), and there was a tendency for the rate to increase as the cell density increased. Notably, the much higher induction rate of PDX1$^+$NKX6.1$^+$ cells (38–40%) was consistently obtained with the S4F-AG cultures, regardless of the size, compared with the S4F-2D cultures.

To validate the mRNA expression of pancreatic bud markers in the S4F-AG cultures (hereafter described as aggregation cultures), we performed qRT-PCR analyses at each time point during Stage 4. The *PDX1* expression was increased in aggregation cultures shortly after the start of Stage 4, while the expression level was not changed in the S4F-2D cultures (hereafter described as monolayer cultures) (Fig. 2D). The expression of pancreatic bud-specific markers, *PTF1A* and *NKX6.1*, also began to increase one day after the start of Stage 4, and progressively increased in aggregation cultures, while the expression in monolayer cultures remained extremely low.

The positive effects of aggregation cultures on the differentiation of pancreatic bud cells were reproduced in multiple hiPSC lines (585A1, 604B1, 648B1, 692D2 and 409B2), in addition to a hESC line, KhES-3 (Fig. 2E). These results suggest that high cell density cultures with cellular aggregation promoted the differentiation of multiple hESC/iPSC cell lines into pancreatic bud cells.

PDX1$^+$NKX6.1$^+$ cells emerge from PDX1^{high} cells in cellular aggregates

In our adhesion culture, we found that there was heterogeneity of the PDX1$^+$ cells in terms of the expression levels (Fig. 1D). We therefore performed flow cytometric analyses of the cell populations in cellular aggregates after 0–20 days of Stage 4 treatments to determine the origin of the NKX6.1$^+$ cells. Before the Stage 4 treatments, around 80% of the cells were PDX1$^+$, and the majority was PDX1^{middle} or PDX1^{low}. However, within one day after the Stage 4 treatments, the majority of the cells became PDX1^{high}. On day 2, the PDX1^{high} cells started to diverge into two populations: one population expressing NKX6.1 and the other showing downregulation of the PDX1 expression (Fig. 3A). The ratio of PDX1$^+$NKX6.1$^+$ cells was significantly increased during the first four to eight days of Stage 4, and reached around 90% on days 12–20 (Fig. 3B). The PDX1$^+$NKX6.1$^+$ cell ratio was similar regardless of the aggregate size (Fig. S2). These results imply that the lineage commitment to PDX1$^+$NKX6.1$^+$ cells occurs between days 2 and 8.

Next, we investigated the localization of PDX1$^+$NKX6.1$^+$ cells in the cellular aggregates. Immunostaining on cryosections of aggregates on days 4 and 12 of Stage 4 revealed that PDX1$^+$NKX6.1$^+$ cells were uniformly distributed inside aggregates (Figs. 4A and B). Notably, most PDX1^{high} cells were PDX1$^+$NKX6.1$^+$ and were co-stained for GATA4 and SOX9, other markers for the pancreatic bud (Jennings et al., 2013). As occurs during *in vivo* pancreatic development, the PDX1$^+$NKX6.1$^+$ cell areas were stratified to become thickened by day 12 (Fig. 4B), suggesting that the increase in the PDX1$^+$NKX6.1$^+$ cell ratio on days 4–20 might be mainly due to the proliferation of these cells. In fact, the total cell numbers were increased by 2-fold on culture day 12 in Stage 4 compared with that observed on days 1–4 (Fig. S3). Insulin$^+$ (INS$^+$) cells were one component of the PDX1$^+$NKX6.1$^-$ cells. These INS$^+$ cells were PDX1^{low}, and some of them were glucagon$^+$ (GCG$^+$). There were some INS$^-$ GCG$^+$ cells, some ghrelin$^+$ (GHR$^+$) cells and some somatostatin$^+$ (SST$^+$) cells, suggesting the lineage commitment into immature fetal endocrine cells (Rezania et al., 2012).

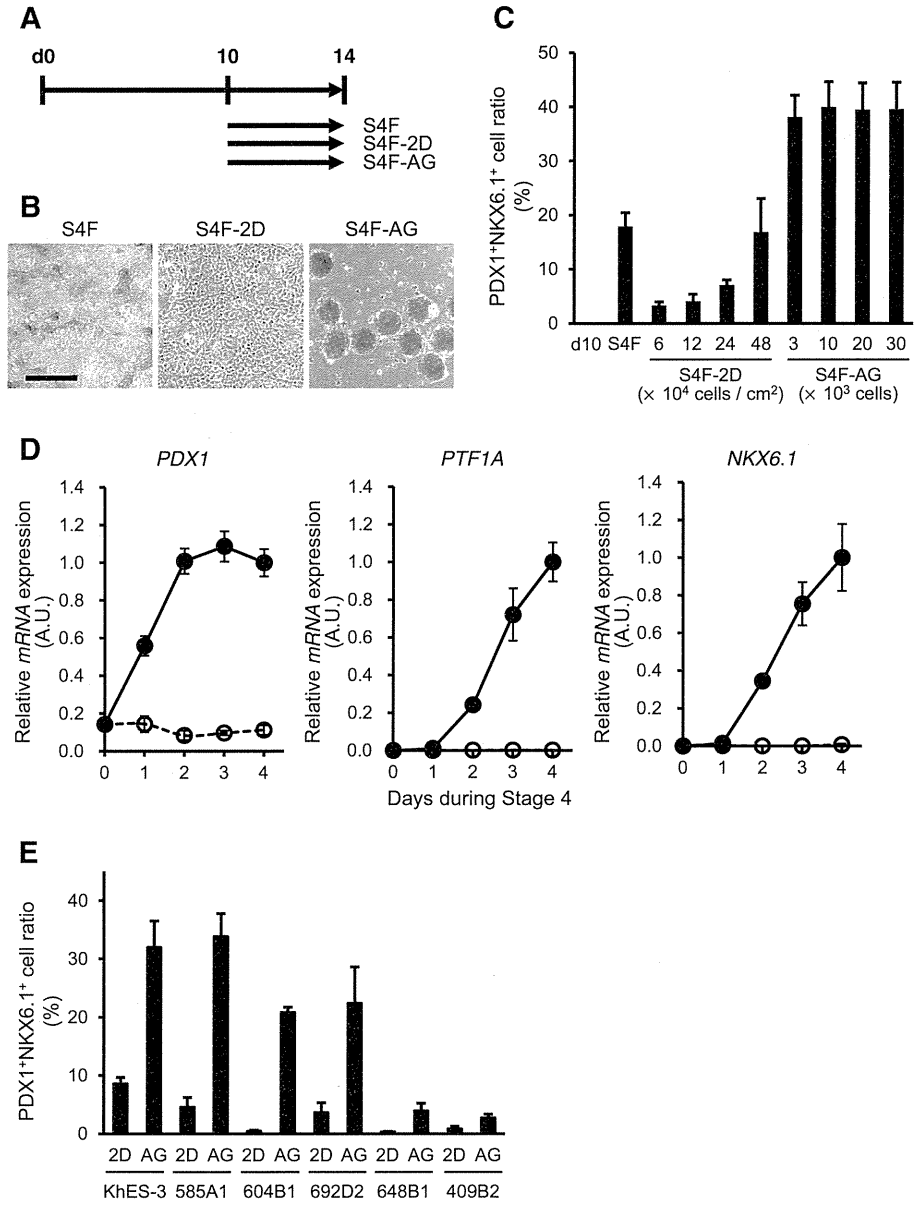

Figure 2 Cell aggregation cultures promote PDX1$^+$NKX6.1$^+$ cell induction from PDX1$^+$ posterior foregut cells. (A) A schematic diagram of the procedures used to assess the effects of the cell density on the cultures with regard to the induction of pancreatic bud cells. Posterior foregut cells differentiated in adhesion cultures were treated with the soluble factors required for pancreatic bud induction (KGF, NOGGIN and EGF), either with only a medium change (S4F) or with re-seeding at different cell densities for monolayer cultures (6–48 × 10^4 cells/cm^2, S4F-2D) or to form cellular aggregates (3–30 × 10^3 cells/aggregate) (S4F-AG). (B) Representative bright field images of the three culture formats. (C) Quantification of the PDX1$^+$NKX6.1$^+$ cell ratio. After the induction of pancreatic bud cells in the three culture conditions described above, cells were examined by flow cytometry. (D) The mRNA expression of pancreatic bud markers, *PDX1*, *PTF1A* and *NKX6.1*, was assessed by quantitative real-time polymerase chain reaction (qRT-PCR) before and during pancreatic bud induction with cell aggregation (black circle, solid line) and in monolayer cultures (open circle, dotted line). The data are presented as the fold-change in gene expression relative to the peak value. (E) A hESC line (KhES-3) and five hiPSC lines (585A1, 604B1, 692D2, 648B1 and 409B2) were differentiated into posterior foregut cells in adhesion cultures. Then, the foregut cells were dissociated, re-seeded either for monolayer cultures (12 × 10^4 cells/cm^2, 2D) or to form cellular aggregates (3 × 10^3 cells/aggregate, AG) and were treated with KGF, NOGGIN and EGF to induce pancreatic bud cells. After the differentiation, the PDX1$^+$NKX6.1$^+$ cell ratio was measured by flow cytometry. The data are presented as the mean ± S.E.M. from three to seven independent experiments in C and from three independent experiments in D and E. Scale bar, 300 μm.

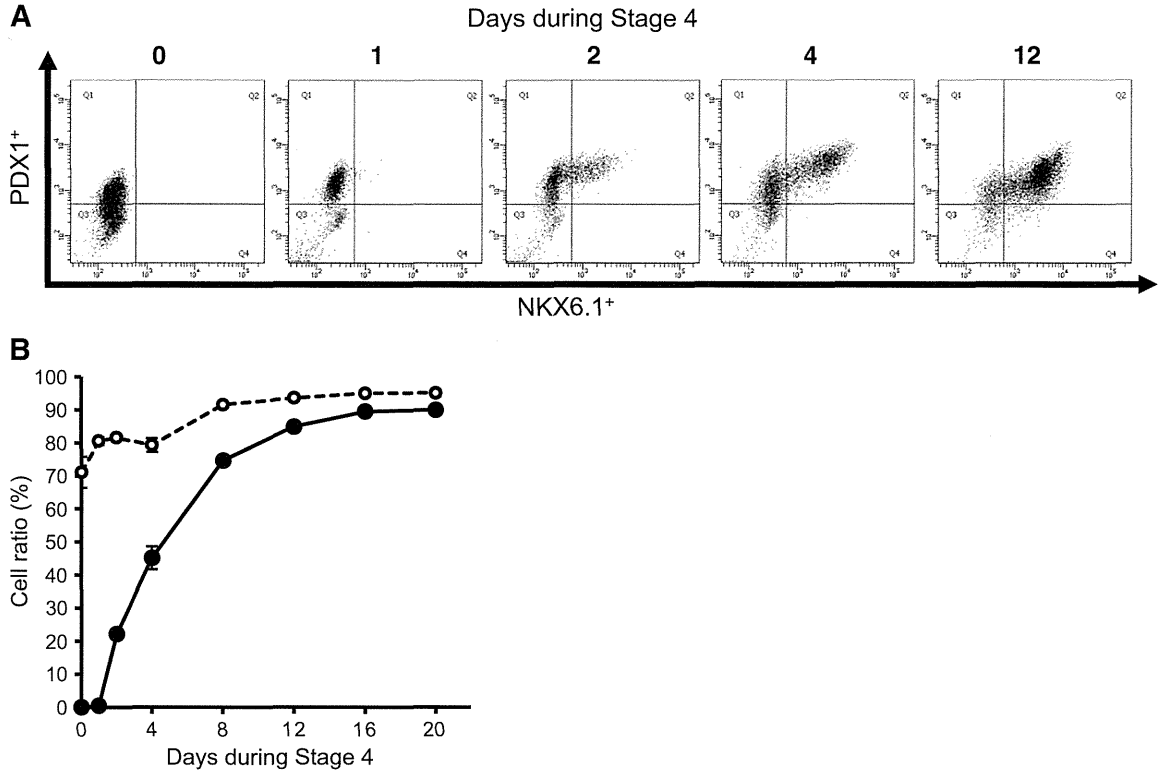

Figure 3 PDX1$^+$NKX6.1$^+$ cells emerge from PDX1^{high} cells in cellular aggregates. Cell populations were analyzed by flow cytometry after 0–20 days of aggregation culture at Stage 4. (A) Representative dot plots indicating that NKX6.1$^+$ cells emerged from PDX1^{high} cells. (B) Quantification of the induction rate of PDX1$^+$NKX6.1$^+$ (black circle, solid line) and the total PDX1$^+$ cells (open circle, dotted line). The data are from three independent experiments presented as the mean ± S.E.M.

The commitment to PDX1$^+$NKX6.1$^+$ cells requires both cell aggregation and soluble factors

A novel protocol combining the treatment with three soluble factors (KGF, NOGGIN and EGF) and cell aggregation cultures was established to efficiently induce the PDX1$^+$NKX6.1$^+$ cells in this study. Three soluble factors were also effective in inducing the *NKX6.1* gene expression in the adhesion cultures (S4F) (Schulz et al., 2012) (Fig. S4). To investigate whether the signals elicited by aggregation cultures were independent of those induced by the three factors, we examined the effects of all combinations of the factors on the *NKX6.1* expression after four-day treatments with aggregation cultures. The cellular aggregates did not express *NKX6.1* without any factor treatments, while the expression was increased by the treatments with each single factor or each combination of two factors out of the three, and the expression was highest when the cells were treated with all three factors (Fig. 5A). These data suggest that the signals elicited by aggregation cultures are independent of those induced by the three factors.

To determine the timing of the soluble factor treatments required for PDX1$^+$NKX6.1$^+$ cell commitment, cellular aggregates were cultured for 12 days, and NOGGIN or all three factors were removed for either the last four or eight days. The removal of NOGGIN did not significantly change the PDX1$^+$NKX6.1$^+$ cell ratio on day 12 (Fig. 5B). On the other hand, the removal of all three factors for the last four or eight days slightly decreased the PDX1$^+$NKX6.1$^+$ cell ratio on day 12, but the ratio was still increased compared to that before the removal. These results suggest that the cell fate commitment into PDX1$^+$NKX6.1$^+$ cells induced by soluble factors occurred by day 4 of Stage 4.

In order to examine whether the selection for PDX1$^+$NKX6.1$^+$ cell progenitors leads to an increase in the ratio of PDX1$^+$NKX6.1$^+$ cells in aggregation cultures, we performed time course analyses of the proliferating and apoptotic cells at Stage 4. The levels of proliferative cells were increased and few cells were apoptotic in the S4F and S4F-2D cultures (Fig. S5). The apoptotic cell ratio tended to be higher in the S4F-AG culture in the early periods of Stage 4 compared with that observed in the S4F and S4F-2D cultures. The apoptotic cell ratio decreased, while the proliferating cell ratio increased, with time in the S4F-AG culture. More apoptotic cells were found among the PDX1$^-$ cells than the PDX1$^+$ cells in the S4F-AG cultures, suggesting that the selection of PDX1$^+$ cells may be a mechanism underlying the increased rate of induction of PDX1$^+$NKX6.1$^+$ cells (Fig. S5D).

PDX1$^+$NKX6.1$^+$ cells differentiate into pancreatic epithelia *in vivo*

We next examined the developmental potential of the PDX1$^+$NKX6.1$^+$ cells generated with aggregation cultures to

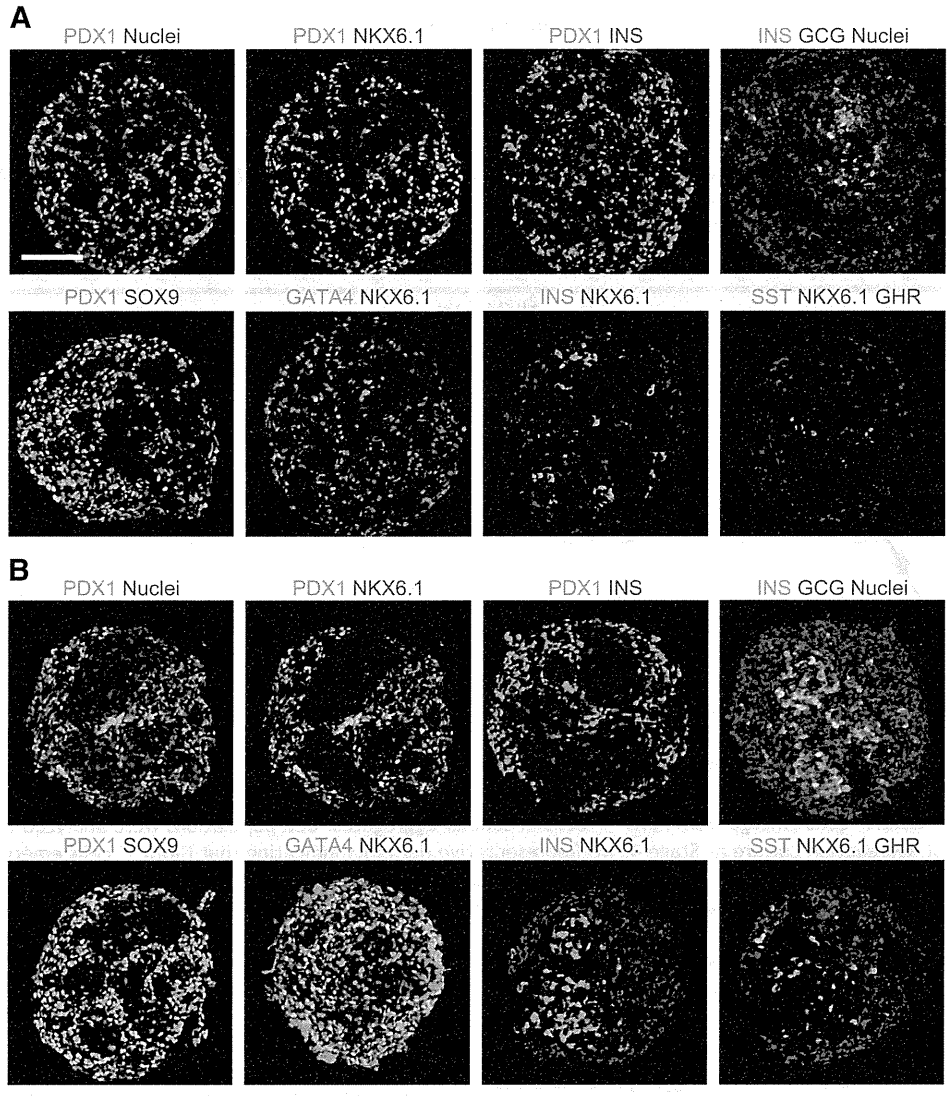

Figure 4 PDX1$^+$NKX6.1$^+$ cells in cellular aggregates co-express multiple pancreatic bud markers. The localization of PDX1$^+$NKX6.1$^+$ cells in aggregates was assessed. Cryosections of cellular aggregates at Stage 4, days 4 (A) and 12 (B), were stained for the indicated markers of pancreatic buds (PDX1, NKX6.1, SOX9 and GATA4) and endocrine cells (INS, GCG, SST and GHR). Pancreatic bud cells were distributed throughout the entire aggregates, and were segregated from endocrine compartments. SOX9, SRY (sex determining region Y)-box9; INS, insulin; GCG, glucagon; SST, somatostatin; GHR, ghrelin. Scale bar, 100 μm.

differentiate into pancreatic cells *in vivo* by implanting the cell aggregates on days 4–5 of Stage 4 into kidney subcapsule of immunocompromised mice. Thirty days after implantation, the aggregates had fused together to become single grafts (Fig. 6A). In contrast to the uniform distribution pattern of PDX1$^+$ cells inside aggregates before implantation (Fig. 4), PDX1$^+$ cells were well-aligned and formed tubular structures, which were observed throughout the entire grafts (Figs. 6B and C). There were INS$^+$ cells budding from tubular structures, as well as endocrine cell clusters (Fig. 6D), which were reminiscent of human embryonic pancreatic epithelia (Riedel et al., 2012). Most INS$^+$ cells were polyhormonal, co-expressing GCG, SST and GHR, without forming islet-like structures or co-expressing NKX6.1, and showed lower PDX1 expression levels compared with the surrounding tubular cells, thus indicating the generation of immature endocrine cells. Some PDX1$^+$ cells were not NKX6.1$^+$ but GATA4$^+$, implying the segregation of endocrine and exocrine lineages. These branched epithelial structures derived from implanted aggregates were observed in three independent experimental cohorts treated with KhES-3 hESCs (seven out of seven mice) and one independent cohort treated with 585A1 hiPSCs (one out of one mouse) (Fig. S6).

To confirm the differentiation potential of PDX1$^+$NKX6.1$^+$ cells into mature pancreatic β-cells, we examined plasma human C-peptide levels in host mice and the response to different blood glucose levels. To obtain a larger number of pancreatic β-cells *in vivo*, cellular aggregates were pre-treated with an ALK5 inhibitor before implantation, since this treatment was previously reported to promote the differentiation into β-cells (Rezania et al., 2012). We found